Ab initio study of high-order harmonic generation of H_2^+ in intense laser fields: Time-dependent non-Hermitian Floquet approach

Dmitry A. Telnov* and Shih-I Chu†

Department of Chemistry, University of Kansas, and Kansas Center for Advanced Scientific Computing, Lawrence, Kansas 66045, USA

(Received 3 August 2004; published 13 January 2005)

We present a *time-dependent* non-Hermitian Floquet approach for the precision three-dimensional nonperturbative calculations of high-order harmonic generation (HHG) rates of the hydrogen molecular ions subject to intense laser fields. The procedure involves an extension of the *complex-scaling generalized pseudospectral* method for nonuniform spatial discretization of the Hamiltonian and non-Hermitian time propagation of the time-evolution operator. The approach is designed for effective and high-precision nonperturbative treatment of high-order multiphoton processes in very intense and/or low-frequency laser fields, which are generally more difficult to treat using the conventional *time-independent* non-Hermitian Floquet matrix techniques. The method is applied to the multiphoton ionization (MPI) and HHG calculations of H_2^+ for the wavelength 532 nm at the equilibrium internuclear separation ($R=2.0$ a.u.) and several laser intensities, as well as at the laser intensity 5×10^{13} W/cm^2 and various internuclear distances in the range between 3.0 and 17.5 a.u. We found that both the MPI and HHG rates are strongly dependent on R. Further, at some internuclear separations R, the HHG productions are strongly enhanced and this phenomenon can be attributed to the resonantly enhanced MPI at these R. Finally, the enhancement of higher harmonics is found to take place mainly at larger R. Detailed study of the correlation between the behavior of MPI and HHG phenomena is presented.

DOI: 10.1103/PhysRevA.71.013408 PACS number(s): 42.50.Hz, 33.80.Rv, 42.65.Ky

I. INTRODUCTION

The exploration of atomic and molecular multiphoton processes in intense laser fields is a subject of much current interest and significance in science and technology [1–3]. In particular, multiple high-order harmonic generation (HHG) is one of the most rapidly developing topics in strong-field atomic physics in the last decade. The generation of harmonics of orders in excess of 300 from rare-gas atoms has been recently demonstrated by several experiments [4,5]. The shortest wavelength generated by the HHG mechanism to date is about 2.7 nm [4,5], well into the water window regime. In the last several years, the study of molecular multiphoton ionization (MPI) and HHG processes has also received considerable attention both experimentally and theoretically. Due to the extra internuclear degree of freedom, the response of molecules to strong fields is considerably more complicated than that of atoms with comparable ionization potential. The exploration of molecular physics in strong fields is only at the beginning stage.

The main aspects of atomic HHG can be explained on the basis of the recollision model [6,7]. According to this model, the atom is first ionized by the laser field. The free electron is accelerated by the field and acquires some additional energy. Oscillating in the field, the electron can return to the core and undergo a recollision. As a result, a recombination can occur, and the extra electron energy is converted into a photon of the harmonic radiation. The model predicts a plateau in the harmonic spectra with the cutoff at approximately $|E_0|+3.17U_P$, where $|E_0|$ is the ionization potential of the atom and U_P is the ponderomotive potential equal to $F^2/(4\omega^2)$, F and ω being the laser field strength and frequency, respectively (linear polarization of the field is assumed). A generalization of this model to the diatomic molecular case was discussed in Ref. [8]. Since molecules are more complex systems than atoms, there exist several topologically different classical orbits that contribute to the harmonic spectra in the recollision model [8]. Additional degrees of freedom as compared to atoms lead to more flexible control of the HHG process. For example, for diatomic molecules one can study the dependence of the HHG spectra on the orientation of the molecular axis and internuclear separation. Recent experiments [9,10] show the possibility of prealigning of molecules in the interaction region.

However, due to the neglect of detailed atomic and molecular structure, the simple recollision model [6–8] and other models [11] based on the Keldysh-Faisal-Reiss approximations, etc., cannot provide quantitative details of the underlying quantum dynamics and HHG spectra. To obtain a full picture, *ab initio* calculations are required. However, *ab initio* time-dependent wave-function calculations of N-electron atomic and molecular systems is beyond the scope of the current supercomputer technology for $N>2$. To overcome this major bottleneck, several self-interaction-free time-dependent density-functional theoretical (TDDFT) approaches, taking into account detailed electronic structure and dynamical electron correlations for atomic [12,13] and diatomic molecular [14,15] systems, have been recently developed. Much remains to be explored along this direction.

Ab initio study of MPI and HHG processes of a hydrogen molecular ion, the simplest two-center molecular system with three electronic degrees of freedom, will be the focus of

*Permanent address: Department of Physics, St. Petersburg State University, 198504 St. Petersburg, Russia; Electronic address: telnov@pcqnt1.phys.spbu.ru

†Electronic address: sichu@ku.edu

this article. Even for H_2^+, accurate three-dimensional (3D) calculations of MPI and HHG rates are by no means straightforward, particularly for the cases of long wavelength and strong laser fields. There are a number of previous H_2^+ calculations (see, for example, Refs. [16–19]), but most of them adopt 1D or 2D model descriptions [16,17] or zero-range potential [8]. Recently, HHG calculations of H_2^+ at the laser wavelength 800 nm were performed using a 3D approach for the time-dependent Schrödinger equation [20]. The results show interesting interference phenomena in the harmonic spectra due to contributions from each nucleus.

Precision calculations of MPI rates of H_2^+ at 1064 nm were accomplished a few years ago [21] by means of the time-independent non-Hermitian Floquet matrix approach [22]. However, such an approach requires the development of a sophisticated numerical procedure for the treatment of ultralarge complex eigenvalue problems [21]. In this paper, we present an alternative *ab initio* approach, the time-dependent non-Hermitian Floquet method, for the high-precision nonperturbative treatment of HHG spectra of the real 3D H_2^+ system. In the present study, we assume the fixed-nuclei approximation (nuclear motion is not taken into account; this is a commonly used approximation in HHG and MPI calculations where the fast electron motion is more important) and the alignment of the molecular axis in the external field direction. We study MPI and HHG in laser fields with the wavelength 532 nm at different laser intensities and internuclear separations R.

We note that although accurate numerical solution of the 3D time-dependent Schrödinger equation of the H_2^+ systems driven by intense laser pulses is now becoming feasible (see, for example, Ref. [21]), high-precision HHG results are generally more difficult to achieve as the harmonic generation rates can vary as much as 10–20 orders of magnitude from low to high harmonics. The primary motivation of the present Floquet study is to provide precision and benchmark HHG results for the monochromatic field case, allowing comprehensive analysis of the R-dependent HHG phenomena in terms of the quasienergy spectrum.

Since HHG is observed in intense laser fields, it is accompanied by multiphoton ionization (MPI). The HHG and MPI processes take place at the same time and are strongly correlated. Thus the investigation of MPI is important for understanding the behavior of HHG spectra. Previous investigations of the ionization dynamics of H_2^+ involved numerical integration of the time-dependent Schrödinger equation [23,24] as well as the time-independent Floquet approach [21,25,26]. Some studies used a quasistatic approach treating the laser field as a static electric field and then averaging over the field strengths within one optical cycle [27,28] (a short review of previous MPI studies is given in Ref. [21]). The applicability of the quasistatic description depends on the wavelength of the laser field. As revealed by the calculations of Ref. [24], for example, at the wavelength 1064 nm the results are consistent with the static tunneling ionization picture, while at 790 nm, large dynamic corrections are observed. Our calculations are performed at even shorter wavelength, 532 nm, where the quasistatic description may not be applicable. Indeed, our results for the ionization rates show strong deviation from the 1064 nm case [21,23,27] and exhibit several sharp resonances as the internuclear separation varies. Analogous behavior of ionization rates was observed in the Floquet study of Ref. [25] at the wavelength 248 nm. We show that the resonances in the MPI process strongly affect the HHG production.

In the present HHG study, we extend the time-dependent non-Hermitian Floquet approach recently developed for the study of the high-order above-threshold multiphoton ionization of atomic systems [29] to the diatomic molecular systems. The approach proved to be very accurate and efficient, particularly for the intense and low-frequency external fields where traditional Floquet Hamiltonian methods have led to very large size matrix problems. In Sec. II, we start with the implementation of the time-dependent non-Hermitian Floquet method for molecular systems in prolate spheroidal coordinates. In Sec. III, we discuss our results for HHG spectra and MPI ionization rates of H_2^+ in the laser field with the wavelength 532 nm. Section IV contains concluding remarks.

II. METHOD

Our time-dependent non-Hermitian Floquet approach consists of the following steps: (i) generalized complex-scaling pseudospectral discretization of the wave function and the Hamiltonian operator in the prolate spheroidal coordinates; (ii) construction of the complex-scaled time-evolution operator for one optical cycle by means of the time propagation using the split-operator technique; (iii) diagonalization of this time-evolution operator which yields the complex quasienergy eigenvalues and corresponding Floquet eigenstates at time moment $t=0$; (iv) time propagation of the selected Floquet states again using the split-operator technique which gives the wave functions on the time grid with uniform spacing within one optical cycle; (v) evaluation of the time-dependent expectation values of the dipole moment, momentum, and acceleration using the computed Floquet wave functions; (vi) Fourier analysis of the above quantities to produce the harmonic generation rates.

A. Pseudospectral discretization in prolate spheroidal coordinates with uniform complex scaling

We make use of the conventional definition of the prolate spheroidal coordinates ξ, η, and φ [30], and the relation between the cylindrical coordinates ρ, z and prolate spheroidal coordinates of the electron is as follows:

$$\rho = a\sqrt{(\xi^2-1)(1-\eta^2)}, \tag{1}$$

$$z = a\xi\eta, \tag{2}$$

$$1 \leqslant \xi < \infty, \quad -1 \leqslant \eta \leqslant 1, \tag{3}$$

a being the half-internuclear distance. The third coordinate, the rotation angle φ about the z axis, is the same for both coordinate systems. The electronic part H_e of the unperturbed Hamiltonian operator of the hydrogen molecular ion H_2^+ can be written as follows in the prolate spheroidal coordinates (atomic units are used):

$$H_e = -\frac{1}{2a^2}\frac{1}{(\xi^2-\eta^2)}\left[\frac{\partial}{\partial\xi}(\xi^2-1)\frac{\partial}{\partial\xi}+\frac{\partial}{\partial\eta}(1-\eta^2)\frac{\partial}{\partial\eta}+\frac{\xi^2-\eta^2}{(\xi^2-1)(1-\eta^2)}\frac{\partial^2}{\partial\varphi^2}\right]+U(\xi,\eta), \tag{4}$$

$U(\xi,\eta)$ being the Coulomb attraction between the electron and the two nuclei,

$$U(\xi,\eta) = -\frac{2\xi}{a(\xi^2-\eta^2)}. \tag{5}$$

The interaction of the electron with the laser field linearly polarized along the z axis is described in the velocity gauge,

$$V(\xi,\eta,t) = i\frac{F}{\omega}\sin\omega t\frac{\partial}{\partial z}+\frac{F^2}{2\omega^2}\sin^2\omega t, \tag{6}$$

where F and ω are the laser field strength and frequency, respectively, and the partial derivative with respect to z is expressed in the prolate spheroidal coordinates as follows:

$$\frac{\partial}{\partial z} = \frac{1}{a(\xi^2-\eta^2)}\left[\eta(\xi^2-1)\frac{\partial}{\partial\xi}+\xi(1-\eta^2)\frac{\partial}{\partial\eta}\right]. \tag{7}$$

The system has the axial symmetry with respect to the z axis, and the projection M of the electron angular momentum on the z axis is conserved. Thus the wave function of the electron $\Psi(\xi,\eta,\varphi,t)$ can be represented in the following form:

$$\Psi(\xi,\eta,\varphi,t) = \Phi(\xi,\eta,t)\exp(iM\varphi), \tag{8}$$

and the coordinate φ is eliminated from the time-dependent Schrödinger equation for the function $\Phi(\xi,\eta,t)$. In what follows, we will limit the discussion to the σ states ($M=0$), and the equation for the function $\Phi(\xi,\eta,t)$ takes the form

$$i\frac{\partial}{\partial t}\Phi(\xi,\eta,t) = [T+U(\xi,\eta)+V(\xi,\eta,t)]\Phi(\xi,\eta,t), \tag{9}$$

where the kinetic energy operator T depends on ξ and η only,

$$T = -\frac{1}{2a^2}\frac{1}{(\xi^2-\eta^2)}\left[\frac{\partial}{\partial\xi}(\xi^2-1)\frac{\partial}{\partial\xi}+\frac{\partial}{\partial\eta}(1-\eta^2)\frac{\partial}{\partial\eta}\right]. \tag{10}$$

Now we are going to apply the Legendre pseudospectral discretization [31] of the wave function and operators in Eq. (9). First, we need to use the mapping transformations, $\xi=\xi(x)$, $\eta=\eta(y)$, to ensure the new quantities x and y span the interval $[-1,1]$. For the pseudoangular coordinate η, the identity transformation is used,

$$\eta(y) = y, \tag{11}$$

while for the pseudoradial coordinate ξ, we apply the complex-scaling mapping transformation,

$$\xi(x) = 1+R_L\frac{1+x}{1-x}\exp(i\alpha), \tag{12}$$

R_L and α being the mapping parameter and complex rotation angle, respectively.

We make use of the Gauss-Legendre abscissas $\{x_i\}$ and $\{y_j\}$ as the collocation points in the pseudospectral discretization. They are defined as the roots of the Legendre polynomials $P_{N_x}(x)$ and $P_{N_y}(y)$, respectively,

$$P_{N_x}(x_i) = 0, \quad P_{N_y}(y_j) = 0. \tag{13}$$

The orders of the polynomials N_x and N_y are equal to the numbers of grid points for the coordinates x and y within the interval $[-1,1]$. The Gauss-Legendre quadrature can be written as follows:

$$\int d^3r\Phi^2 = 2\pi a^3\sum_{i=1}^{N_x}\sum_{j=1}^{N_y}\phi_{ij}^2, \tag{14}$$

where ϕ_{ij} are related to the values of the function Φ at the collocation points,

$$\Phi(\xi(x_i),\eta(y_j),t) = \sqrt{\frac{(1-x_i^2)(1-y_j^2)}{\xi_i'\eta_j'(\xi_i^2-\eta_j^2)}}P_{N_x}'(x_i)P_{N_y}'(y_j)\phi_{ij}. \tag{15}$$

In Eq. (15), the primes denote the derivatives of the functions with respect to their arguments. The discretized kinetic energy and $\partial/\partial z$ operators are matrices of the order $N_xN_y\times N_xN_y$. They have the following matrix elements as acting on the vector $\{\phi_{ij}\}$:

$$T_{ij;i'j'} = \sqrt{\frac{(1-x_i^2)(1-y_j^2)(1-x_{i'}^2)(1-y_{j'}^2)}{\xi_i'\eta_j'\xi_{i'}'\eta_{j'}'(\xi_i^2-\eta_j^2)(\xi_{i'}^2-\eta_{j'}^2)}}\times\frac{1}{2a^2}\left[\delta_{jj'}\frac{\eta_j'}{1-y_j^2}\sum_{k=1}^{N_x}\frac{1}{\xi_k'}\frac{\xi_k^2-1}{1-x_k^2}D_{ki}^{(x)}D_{ki'}^{(x)}+\delta_{ii'}\frac{\xi_i'}{1-x_i^2}\sum_{k=1}^{N_y}\frac{1}{\eta_k'}\frac{1-\eta_k^2}{1-y_k^2}D_{kj}^{(y)}D_{kj'}^{(y)}\right], \tag{16}$$

$$\left(\frac{\partial}{\partial z}\right)_{ij;i'j'} = \sqrt{\frac{(1-x_i^2)(1-y_j^2)(1-x_{i'}^2)(1-y_{j'}^2)}{\xi_i'\eta_j'\xi_{i'}'\eta_{j'}'(\xi_i^2-\eta_j^2)(\xi_{i'}^2-\eta_{j'}^2)}}\times\frac{1}{2a}\left[\delta_{jj'}\frac{\eta_j'\eta_j}{1-y_j^2}\left(\frac{\xi_i^2-1}{1-x_i^2}D_{ii'}^{(x)}-\frac{\xi_{i'}^2-1}{1-x_{i'}^2}D_{i'i}^{(x)}\right)+\delta_{ii'}\frac{\xi_i'\xi_i}{1-x_i^2}\left(\frac{1-\eta_j^2}{1-y_j^2}D_{jj'}^{(y)}-\frac{1-\eta_{j'}^2}{1-y_{j'}^2}D_{j'j}^{(y)}\right)\right]. \tag{17}$$

The first derivative matrices $D_{ii'}^{(x)}$, $D_{jj'}^{(y)}$ have simple analytical expressions in the pseudospectral method; for the sets of the Gauss-Legendre collocation points, they appear as follows:

$$D_{ii'}^{(x)} = \frac{1}{x_i-x_{i'}}, \quad i\neq i'; \quad D_{ii}^{(x)} = \frac{x_i}{1-x_i^2}; \tag{18}$$

$$D_{jj'}^{(y)} = \frac{1}{y_j-y_{j'}}, \quad j\neq j'; \quad D_{jj}^{(y)} = \frac{y_j}{1-y_j^2}. \tag{19}$$

As for the Coulomb potential $U(\xi,\eta)$ on the right-hand side of Eq. (9), it is represented by a diagonal matrix (like any

multiplication operator in the pseudospectral method), with the matrix elements $U(\xi(x_i),\eta(y_j))\delta_{ii'}\delta_{jj'}$. Equations (15)–(19) are the main results of the current Gauss-Legendre pseudospectral discretization in the prolate spheroidal coordinates. We should note that previously a pseudospectral discretization scheme in the prolate spheroidal coordinates was developed in Ref. [21]. However, that approach used a different definition of the prolate spheroidal coordinates and a different (Gauss-Lobatto) set of collocation points. The advantage of these methods is that they allow nonuniform and optimal spatial grid discretization (denser mesh near each nucleus and sparser mesh at larger electron-nucleus separations). This improves greatly both the accuracy and the efficiency of the electronic structure and time-dependent calculations.

B. Complex-scaled time-evolution operator

If Eq. (9) is solved for the Floquet state, the wave function $\Phi(\xi,\eta,t)$ can be expanded in the time Fourier series,

$$\Phi(\xi,\eta,t)=\exp(-i\varepsilon t)\sum_{m=-\infty}^{\infty}\exp(-im\omega t)\Phi_m(\xi,\eta), \quad (20)$$

where ε is a complex quasienergy with the real part representing the ac Stark-shifted energy level of the system, and the imaginary part is equal to minus one-half of the ionization rate. Then Eq. (9) is equivalent to the infinite-dimension time-independent matrix eigenvalue problem for the quasienergy and the vector of the Fourier components Φ_m,

$$[H_0-m\omega]\Phi_m+\sum_{m'}V_{m-m'}\Phi_{m'}=\varepsilon\Phi_m, \quad (21)$$

$$-\infty<m<\infty,$$

where

$$H_0=T+U(\xi,\eta) \quad (22)$$

is the unperturbed molecular electronic Hamiltonian, and V_m are the time Fourier components of the interaction operator $V(\xi,\eta,t)$. The left-hand side of Eq. (21) represents the time-independent Floquet Hamiltonian acting on the vector of the wave-function Fourier components Φ_m. In practical computations, the set of Eq. (21) is truncated, and the Floquet Hamiltonian matrix has a finite dimension. However, this dimension $[N_xN_yN_m\times N_xN_yN_m$, where N_m is the number of equations retained in the set (21)] can be very large, particularly for strong and low-frequency external fields.

An alternative way [29] to solve for Floquet wave functions is by the extension of the time-evolution operator approach [22,32,33]. Consider the one-optical-cycle time-evolution operator U_T. For the Floquet wave function $\Phi(\xi,\eta,t)$, the following equation holds:

$$U_T\Phi(\xi,\eta,0)=\exp(-i\varepsilon T)\Phi(\xi,\eta,0). \quad (23)$$

Equation (23) is an eigenvalue problem for the time-evolution operator U_T. The quasienergy can be determined from the eigenvalue $\exp(-i\varepsilon T)$. Unlike Eq. (21), there are no time Fourier components in Eq. (23), and the matrix dimension is $N_xN_y\times N_xN_y$ only. The penalty for the reduced matrix size is some extra work required to obtain the one-cycle propagator U_T.

At the time moment t, the time-evolution operator U_t satisfies the equation

$$i\frac{\partial}{\partial t}U_t=[H_0+V(\xi,\eta,t)]U_t \quad (24)$$

with the initial condition at $t=0$,

$$U_0=\mathbb{I}, \quad (25)$$

where $\mathbb{I}$ is the identity operator. Upon integration of Eq. (24) from $t=0$ to $t=T$, one obtains the one-cycle propagator U_T. We employ the following split-operator, second-order short-time propagation formula,

$$U_{t+\Delta t}\simeq\exp(-i\tfrac{1}{2}\Delta tH_0)\exp\left(-i\Delta tV(\xi,\eta,t+\tfrac{1}{2}\Delta t)\right)\times\exp(-i\tfrac{1}{2}\Delta tH_0)U_t. \quad (26)$$

The smaller Δt, the more accurate Eq. (26), and the error is of the order $O[(\Delta t)^3]$. The one-cycle time-evolution operator U_T is calculated by sequentially applying Eq. (26), starting from $t=0$. To facilitate the computations for the velocity gauge interaction $V(\xi,\eta,t)$ (6), the time propagation according to Eq. (26) is performed in the momentum space where the operator $V(\xi,\eta,t)$ is diagonal.

The matrix $\exp\left(-i\frac{1}{2}\Delta tH_0\right)$ is computed only once for the specified Δt and can be represented by the spectral expansion. Since the matrix H_0 is non-Hermitian, there are two sets of eigenvectors, the right eigenvectors $\{\psi_k^R\}$ and the left eigenvectors $\{\psi_k^L\}$, involved in the spectral expansion [29],

$$\exp\left(-i\frac{1}{2}\Delta tH_0\right)=\sum_{k=1}^{N_xN_y}\exp\left(-i\frac{1}{2}\Delta tE_k\right)|\psi_k^R\rangle\langle\psi_k^L|. \quad (27)$$

The eigenvectors ψ_k^R and ψ_k^L correspond to the same complex eigenvalue E_k and satisfy the biorthogonality and binormalization relations,

$$\langle\psi_{k'}^L|\psi_k^R\rangle=0, \quad k\neq k', \quad (28)$$

$$\langle\psi_k^L|\psi_k^R\rangle=1. \quad (29)$$

The time-dependent matrix $\exp\left(-i\Delta tV(\xi,\eta,t+\frac{1}{2}\Delta t)\right)$ must be computed at each time step, but this operation is fast since this part of the short-time propagator is diagonal in the momentum representation used in the present calculations, since the interaction is described in the velocity gauge.

The above procedure describes a complex-scaling approach to the *eigenvalue* problem for the one-cycle time-evolution operator. The computed operator U_T is being diagonalized to produce the complex quasienergy and the corresponding Floquet state at $t=0$. The first implementation of this method was accomplished in Ref. [29] for the study of the high-order above-threshold multiphoton detachment of H^-. Note that previously the complex-scaling approaches in time-propagation schemes were applied to the *initial-state* problems [34,35].

C. Time-dependent non-Hermitian Floquet approach for the calculation of HHG spectra

Once the one-cycle time-evolution operator U_T is constructed and diagonalized to produce the desired Floquet state with the quasienergy ε and the (right) wave function $\Phi^R(\xi,\eta,0)$, the latter is used as a starting point for the time-propagation process based on the same split-operator formula (26). As a result, the right wave function $\Phi^R(\xi,\eta,t)$ is obtained on the uniform time grid between $t=0$ and $t=T$. This wave function is used to calculate the time-dependent dipole moment $D(t)$, momentum $P(t)$, and acceleration $A(t)$ expectation values. Actually, to calculate those expectation values one needs also the left wave function $\Phi^L(\xi,\eta,t)$, so the following expressions can be used:

$$D(t) = \langle \Phi^L(\xi,\eta,t)|z|\Phi^R(\xi,\eta,t)\rangle, \tag{30}$$

$$P(t) = -i\left\langle \Phi^L(\xi,\eta,t)\left|\frac{\partial}{\partial z}\right|\Phi^R(\xi,\eta,t)\right\rangle, \tag{31}$$

$$A(t) = \left\langle \Phi^L(\xi,\eta,t)\left|\frac{\partial}{\partial z}U(\xi,\eta)\right|\Phi^R(\xi,\eta,t)\right\rangle + F\cos\omega t. \tag{32}$$

The right and left wave functions satisfy the time-dependent equations

$$i\frac{\partial}{\partial t}|\Phi^R(\xi,\eta,t)\rangle = H(t)|\Phi^R(\xi,\eta,t)\rangle, \tag{33}$$

$$-i\frac{\partial}{\partial t}\langle\Phi^L(\xi,\eta,t)| = \langle\Phi^L(\xi,\eta,t)|H(t), \tag{34}$$

where H is the total non-Hermitian Hamiltonian matrix,

$$H = H_0 + V(\xi,\eta,t). \tag{35}$$

For the uniform complex scaling, the following relation holds for this matrix:

$$H^T(-t) = H(t), \tag{36}$$

where the superscript T denotes the transposed matrix. As a consequence, the right and left time-dependent wave functions are related as

$$[\Phi^L(\xi,\eta,t)]^* = \Phi^R(\xi,\eta,-t) = \exp(i\varepsilon T)\Phi^R(\xi,\eta,T-t). \tag{37}$$

That is why one can evaluate the expressions (30)–(32) using the right wave functions only.

It can be easily verified that the expectation values of the dipole moment, momentum, and acceleration satisfy the following equations:

$$\frac{d}{dt}D(t) = P(t) - \frac{F}{\omega}\sin\omega t, \tag{38}$$

$$\frac{d^2}{dt^2}D(t) = A(t). \tag{39}$$

The nth-order harmonic generation rates Γ_n (the number of photons with the frequency $n\omega$ emitted per unit time) are calculated according to the classical electrodynamics formula

$$\Gamma_n = \frac{4|A_n|^2}{3n\omega c^3}, \tag{40}$$

where c is the speed of light and A_n is the Fourier component of the acceleration $A(t)$,

$$A_n = \frac{1}{T}\int_0^T dt\,\exp(in\omega t)A(t). \tag{41}$$

Equation (40) represents the so-called acceleration form of the HHG rates expression. The dipole and momentum forms can be obtained using the relations between A_n and Fourier components of the dipole moment and momentum, D_n and P_n,

$$A_n = -n^2\omega^2 D_n, \tag{42}$$

$$A_n = -in\omega P_n - \tfrac{1}{2}F[\delta_{n,1} + \delta_{n,-1}]. \tag{43}$$

III. RESULTS AND DISCUSSION

To test the quality of the wave functions obtained by the present time-dependent non-Hermitian Floquet approach, we performed the calculations of the harmonic spectra using three different forms for the harmonic generation rates expressions: the dipole form, the momentum form, and the acceleration form. If the exact wave functions are used, all three forms should yield the same result. However, if the wave functions are approximate, one expects some discrepancies when employing different formulas for the harmonic generation rates. The results of the calculations are presented in Tables I and II for the laser field intensities 5×10^{13} and 1×10^{14} W/cm^2, respectively. As one can see, an excellent agreement exists for a wide interval of harmonic orders starting from the lowest third harmonic and ending well beyond the cutoff and covers a 15 orders of magnitude range in the HHG rates. To our knowledge, these are the first precision *ab initio* calculations of high-order harmonic generation by the hydrogen molecular ion that have achieved full convergence of the HHG spectra.

We present two sets of the HHG spectra calculations. In these calculations, we used the momentum form of the expression for the HHG rates. In the first set, we have computed the harmonic generation rates at the internuclear separation $R=2$ a.u. and several laser field intensities. To achieve convergence in the time-evolution operator and wave-function computations for the highest intensity 5×10^{14} W/cm^2, we applied 80 pseudoradial and 20 pseudoangular grid points and used 65 536 time-propagation steps. For the lowest intensity 5×10^{13} W/cm^2, 60 pseudoradial, 20 pseudoangular grid points, and 32 768 time-

TABLE I. HHG rates of H_2^+ in the ground electronic $(1\sigma_g)$ state for the internuclear separation $R=2$ a.u. The laser field wavelength is 532 nm and the intensity is 5×10^{13} W/cm^2. Shown are the results of the calculations using the dipole (D), momentum (P), and acceleration (A) forms of the HHG rates expression. N is the order of the harmonic. The numbers in brackets indicate the powers of 10.

	HHG rates (a.u.)		
N	D	P	A
3	2.85[−17]	2.85[−17]	2.89[−17]
5	1.65[−16]	1.65[−16]	1.65[−16]
7	4.84[−21]	4.84[−21]	4.86[−21]
9	9.74[−22]	9.74[−22]	9.78[−22]
11	3.98[−21]	3.98[−21]	3.99[−21]
13	4.87[−22]	4.88[−22]	4.92[−22]
15	4.17[−22]	4.17[−22]	4.17[−22]
17	5.42[−23]	5.42[−23]	5.42[−23]
19	2.11[−24]	2.11[−24]	2.11[−24]
21	2.56[−26]	2.56[−26]	2.56[−26]
23	1.24[−28]	1.24[−28]	1.24[−28]
25	2.94[−31]	2.94[−31]	2.94[−31]

propagation steps were enough to obtain fully converged results.

The results are presented in Fig. 1. As may be expected, for higher laser intensities the harmonic spectrum becomes wider with the cutoff position shifted towards higher harmonics. It is instructive to compare the behavior of the HHG spectrum obtained from the present accurate Floquet calculations with the qualitative predictions of the classical "simple man's model" [8]. According to this model, for the two-center system, there exist topologically different classical electron trajectories which can lead to collisions with the nuclei and emission of high-energy photons. Besides the collision with the parent core which resembles the single atom case and leads to the harmonic spectrum cutoff position at the energy $|E_0|+3.17U_p$ irrespective of the laser field intensity and internuclear separation, the collisions can occur also with the other nucleus. In the latter case, the return kinetic energy of the electron depends on the field intensity and frequency as well as on the distance between the nuclei. For the field parameters used in the present calculations, two different classical trajectories may be responsible for the high kinetic energy of the electron when it returns to the other nucleus. The corresponding maximal recombination energies appear quite close to the atomic one and are listed in Table III for the intensities used in the calculations. All three values which mark the harmonic spectrum cutoff position are also shown by arrows in Fig. 1. For the highest intensity used in the calculations, 5×10^{14} W/cm^2, the plateau in the HHG spectrum is wide (extends to the harmonic order 33) and exhibits maxima in the dependence on the harmonic order. One of them is located just before the cutoff and corresponds to the classical trajectories discussed above. The other maxima can be attributed to collisions with the parent and other nucleus after the return at larger times (more than one period of the field). For example, the next two extrema in the dependence of the recombination energy on the initial time correspond to $|E_0|+1.49U_p$ and $|E_0|+1.60U_p$, or 21.5ω and 22.2ω, which is in fair agreement with the position of the next maximum in the HHG spectrum.

The "simple man's model" also predicts a maximum in the low-energy part of the HHG spectrum, corresponding to the harmonic order FR/ω (the so-called "low-energy hump" [8]). At the internuclear separation $R=2$ a.u. and laser wave-

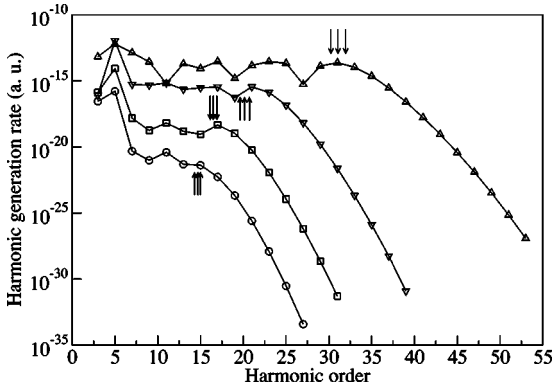

FIG. 1. HHG rates of H_2^+ in the ground $(1\sigma_g)$ electronic state at the internuclear separation $R=2$ a.u. The wavelength of the laser field used is 532 nm and the intensities are 5×10^{13} W/cm^2 (circles), 1×10^{14} W/cm^2 (squares), 2×10^{14} W/cm^2 (triangles down), and 5×10^{14} W/cm^2 (triangles up). The arrows indicate the positions of maximum return kinetic energies of the electron as follows from the "simple man's model" [8].

TABLE II. HHG rates of H_2^+ in the ground electronic $(1\sigma_g)$ state for the internuclear separation $R=2$ a.u. The laser field wavelength is 532 nm and the intensity is 1×10^{14} W/cm^2. Shown are the results of the calculations using the dipole (D), momentum (P), and acceleration (A) forms of the HHG rates expression. N is the order of the harmonic. The numbers in brackets indicate the powers of 10.

	HHG rates (a.u.)		
N	D	P	A
3	1.33[−16]	1.33[−16]	1.36[−16]
5	8.71[−15]	8.71[−15]	8.72[−15]
7	1.50[−18]	1.50[−18]	1.50[−18]
9	1.79[−19]	1.79[−19]	1.79[−19]
11	6.56[−19]	6.56[−19]	6.57[−19]
13	1.53[−19]	1.53[−19]	1.53[−19]
15	9.20[−20]	9.20[−20]	9.20[−20]
17	4.61[−19]	4.61[−19]	4.61[−19]
19	1.08[−19]	1.08[−19]	1.08[−19]
21	5.74[−21]	5.74[−21]	5.74[−21]
23	1.16[−22]	1.16[−22]	1.16[−22]
25	1.15[−24]	1.15[−24]	1.15[−24]
27	6.46[−27]	6.45[−27]	6.45[−27]
29	2.28[−29]	2.25[−29]	2.24[−29]

TABLE III. Cutoff positions of the harmonic spectrum at internuclear separation 2 a.u. as follows from the "simple man's model" [8] for the field parameters used in the present calculations.

Laser field intensity (W/cm^2)	Maximum recombination energies
5×10^{13}	$\|E_0\|+2.72U_p=14.3\omega$
	$\|E_0\|+3.17U_p=14.7\omega$
	$\|E_0\|+3.68U_p=15.0\omega$
1×10^{14}	$\|E_0\|+2.85U_p=16.1\omega$
	$\|E_0\|+3.17U_p=16.5\omega$
	$\|E_0\|+3.53U_p=16.9\omega$
2×10^{14}	$\|E_0\|+2.94U_p=19.6\omega$
	$\|E_0\|+3.17U_p=20.2\omega$
	$\|E_0\|+3.42U_p=20.7\omega$
5×10^{14}	$\|E_0\|+3.02U_p=30.2\omega$
	$\|E_0\|+3.17U_p=31.1\omega$
	$\|E_0\|+3.33U_p=32.0\omega$

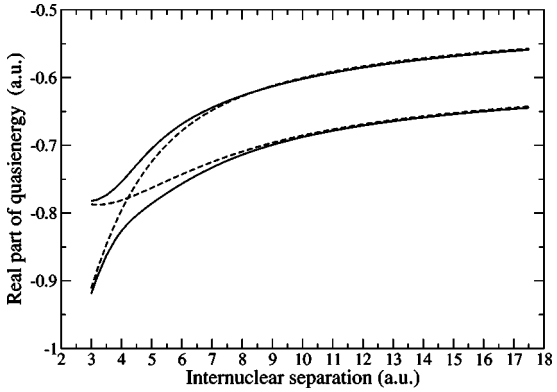

FIG. 2. Real parts of the complex quasienergies for the lower and upper Floquet states as functions of internuclear separation R (solid lines). The dashed lines show the unperturbed energies $E(1\sigma_g)$ and $E(1\sigma_u)-\omega$ (diabatic curves that exhibit a crossing at $R\approx4.2$ a.u.). The photon energy $\omega=0.085\,645\,4$ a.u. corresponds to the wavelength 532 nm, and the laser field intensity is 5×10^{13} W/cm^2.

length 532 nm, however, the position of this maximum is below the third harmonic, even for the highest intensity 5×10^{14} W/cm^2 used in the calculations. That is why the low-energy hump is not well pronounced in the present HHG spectra. Probably, the maximum in the calculated HHG spectra at the fifth harmonic can be attributed to this feature of the classical analysis.

In the second set of the calculations, we computed the harmonic generation rates at the intensity 5×10^{13} W/cm^2 for various internuclear distances between 3 and 17.5 a.u. The two lowest-lying unperturbed states of H_2^+—$1\sigma_g$ and $1\sigma_u$—become nearly degenerate at larger internuclear separations. Thus in our Floquet calculations we need to compute two Floquet states which are dominated by the unperturbed $1\sigma_g$ and $1\sigma_u$ states. We shall call them the lower state and the upper state. For the laser field with the wavelength 532 nm, a one-photon resonance ($\omega=0.085\,645\,4$ a.u.) occurs at the internuclear distance R approximately equal to 4 a.u. The $1\sigma_g$ and $1\sigma_u$ states are strongly mixed in the lower and upper Floquet states in the vicinity of this resonance. For the internuclear separations R less than 4 a.u., the lower Floquet state is dominated by $1\sigma_g$ unperturbed state, and the upper Floquet state is dominated by the $1\sigma_u$ unperturbed state. The situation is reversed for the internuclear separations larger than 4 a.u. The real parts of the quasienergies for the lower and upper states as functions of R undergo an avoided crossing at this distance (see Fig. 2).

The HHG spectra demonstrate strong dependence on the internuclear separation R. In Fig. 3, we show the HHG rates for $R=3$, 6, 10, and 16 a.u. for both the upper and the lower Floquet states, respectively. As one can see, for the same harmonic order n the difference between the values of Γ_n at different R can be as large as several orders of magnitude. Higher-order harmonics (15th and above) are generally enhanced at the larger internuclear distances shown, for example 16 a.u. There is no regular dependence on R for the lower-order harmonics. Our calculations reveal a strong correlation between the ionization rates and harmonic generation rates. In Fig. 4, we show the ionization rates of the H_2^+ lower and upper Floquet states as a function of R. When the internuclear distance varies from $R=3$ a.u. to $R=17.5$ a.u., the ionization potentials for the unperturbed $1\sigma_g$ and $1\sigma_u$ electronic states of H_2^+ change from 0.911 to 0.557 and from 0.701 to 0.557 atomic units, respectively. Several multiphoton ionization thresholds exist within this range of R, as the minimum number of photons required for ionization (in the weak-field limit) changes from 11 to 7 for the $1\sigma_g$ state, and from 9 to 7 for the $1\sigma_u$ state. However, the correct position of the thresholds in the strong laser field must be determined from the quasienergies rather than unperturbed energies, and the ponderomotive shift of the continuum onset should be taken into account. Thus for the lower Floquet state, the ionization thresholds are located approximately at 3.2, 4.4, and 7.5 a.u; for the upper Floquet state, the ionization threshold positions are at 4.6 and 7.4 a.u. With R increasing, the next (and the last) thresholds appear at 19.6 a.u. for both the lower and upper Floquet states; these last thresholds are be-

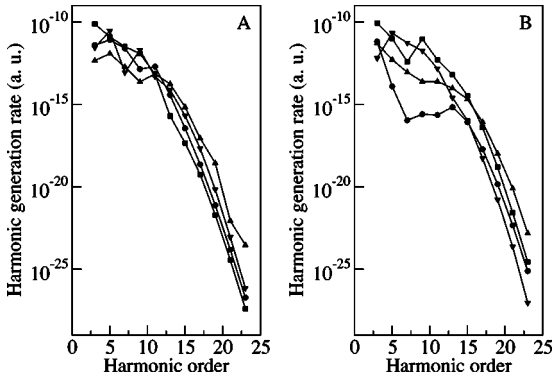

FIG. 3. HHG rates of H_2^+ in the upper (A) and lower (B) Floquet states at several internuclear separations R: $R=3$ a.u. (circles), $R=6$ a.u. (squares), $R=10$ a.u. (triangles down), and $R=16$ a.u. (triangles up). The wavelength of the laser field is 532 nm and the intensity is 5×10^{13} W/cm^2.

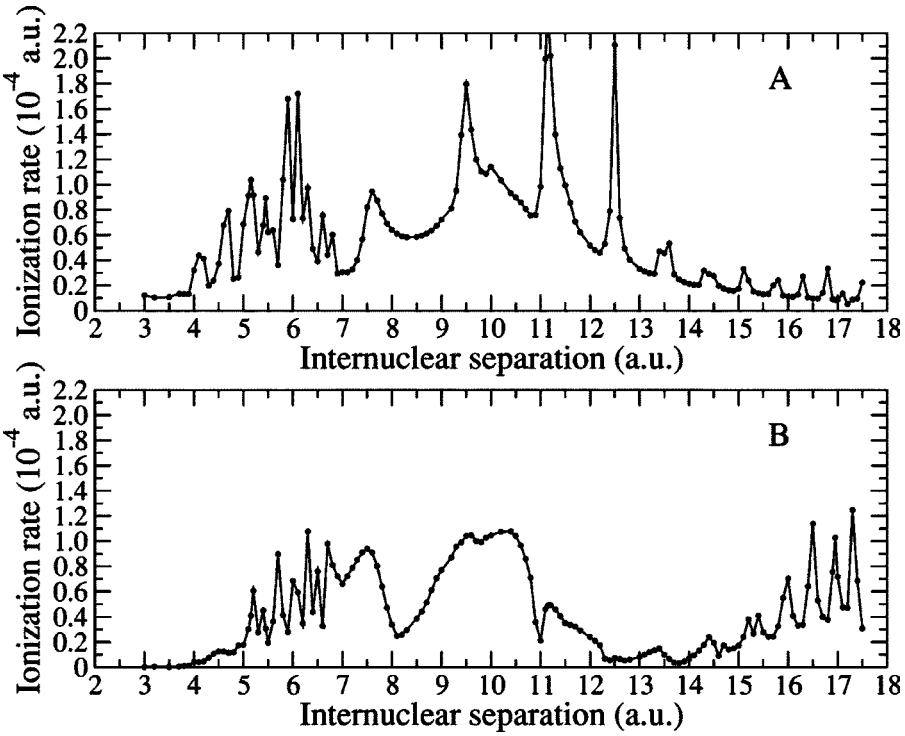

FIG. 4. Multiphoton ionization rates of H_2^+ in the upper (A) and lower (B) Floquet states vs the internuclear separation R showing the resonance-enhanced pattern at several R. The wavelength of the laser field is 532 nm and the intensity is 5×10^{13} W/cm^2.

yond the R range where the present calculations were performed, however.

When going from smaller to higher internuclear separations and approaching the next threshold, a series of resonances with the excited electronic states of H_2^+ is encountered which causes a significant enhancement in the ionization process. In Fig. 4, such a resonance series is clearly seen around 6 a.u. Another large resonance series is spread from 9 to 17.5 a.u. Analogous resonances in the ionization rate as a function of the internuclear separation were

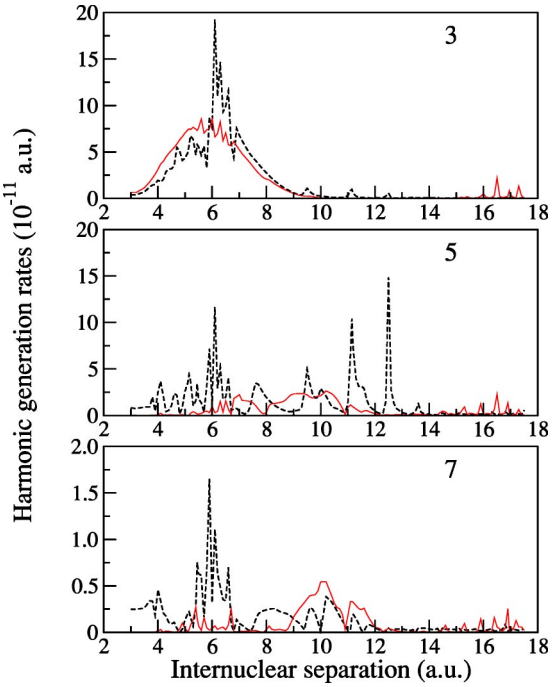

FIG. 5. (Color online) Harmonic generation rates of H_2^+ in the upper (dashed line) and lower (solid line) Floquet states vs the internuclear separation R. Shown are the harmonics 3 to 7; the harmonic order is labeled in each graph. The wavelength of the laser field is 532 nm and the intensity is 5×10^{13} W/cm^2.

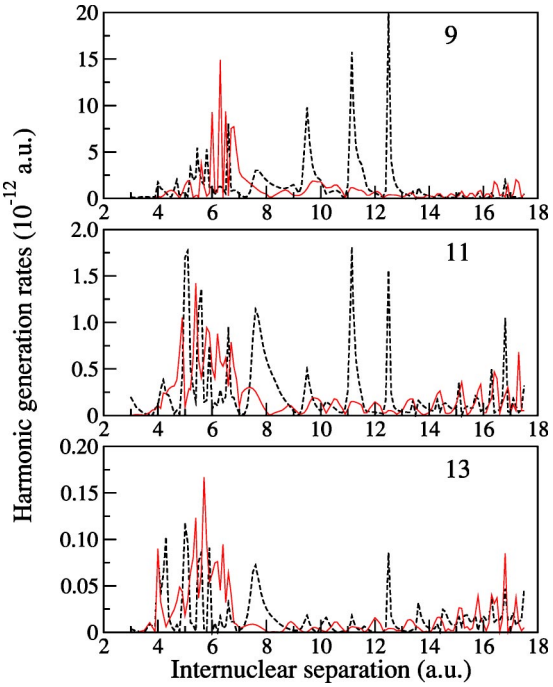

FIG. 6. (Color online) Harmonic generation rates of H_2^+ in the upper (dashed line) and lower (solid line) Floquet states vs the internuclear separation R. Shown are the harmonics 9 to 13; the harmonic order is labeled in each graph. The wavelength of the laser field is 532 nm and the intensity is 5×10^{13} W/cm^2.

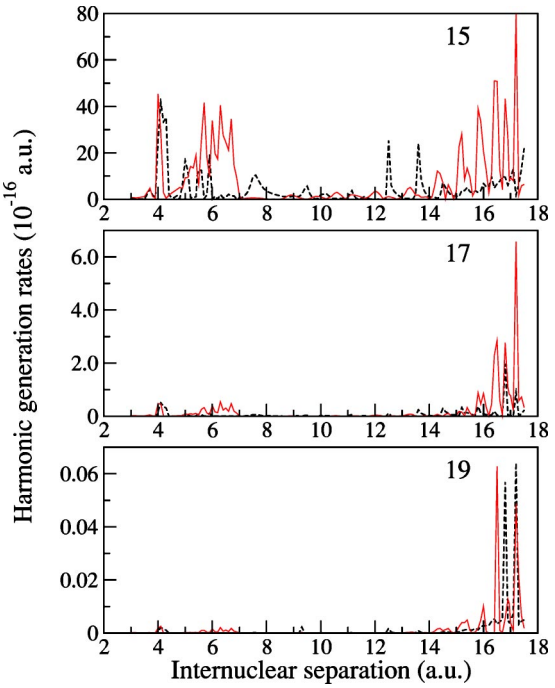

FIG. 7. (Color online) Harmonic generation rates of H_2^+ in the upper (dashed line) and lower (solid line) Floquet states vs the internuclear separation R. Shown are the harmonics 15 to 19; the harmonic order is labeled in each graph. The wavelength of the laser field is 532 nm and the intensity is 5×10^{13} W/cm^2.

revealed in the previous Floquet calculations by Madsen, Plummer, and McCann [25,26] at shorter wavelengths 248 nm and 212 nm.

The resonant enhancement of ionization occurs for both the lower and upper Floquet states. However, for the upper state the ionization rate is generally larger than that for the lower state (except for the internuclear separations larger than 15 a.u.). The upper state is dominated by the (even) $1\sigma_g$ unperturbed state at $R>4$ a.u. Thus it has a significant population between the nuclei which is easier to ionize, as discussed by Codling and Frasinski [36]. On the contrary, the lower state is dominated by the odd $1\sigma_u$ state, and the population between the nuclei is suppressed.

At the very large internuclear separations ($R>15$ a.u.), the ionization rate of the lower Floquet state exceeds that of the upper state. At such large distances, one can expect a transition to the separated atoms picture which features the interference of the contributions from the two atoms to the total ionization rate for the both Floquet states. As a consequence, the ionization rate exhibits an oscillatory behavior as a function of R. The minima of the ionization rate for the upper state must correspond to the maxima for the lower state, and vice versa. One can roughly estimate the period of the interference oscillations ΔR from the equation $k\Delta R=2\pi$, where k is the average momentum of the electron in the continuum. Since the laser field intensity used in these calculations is not very high (5×10^{13} W/cm^2), a reasonable value of k can be the momentum of the electron after absorption of the minimal number of photons required for ionization, that is, $k\approx\sqrt{2\omega}$. Then $\Delta R\approx15$ a.u., and the separation between the adjacent interference minimum and maximum is approximately 7.5 a.u. For larger average electron momentum k, ΔR becomes smaller, but anyway one can expect the period of the interference oscillations to be of the order of a few atomic units, which is much larger than the separation between the adjacent resonance peaks in the ionization rate dependence on R. One can see the beginning of this interference oscillatory structure in Fig. 4 at the internuclear separations larger than 14–15 a.u.

The resonances in the ionization process strongly affect the harmonic generation as well. In Figs. 5–7, we show the HHG rates for the harmonics 3–19 as a function of R. As one can see, the enhancement in the harmonic generation occurs exactly at those internuclear distances where the ionization rates show resonances. The production of low-order harmonics rates is increased in the region around $R=6$ a.u. The three high ionization peaks of the upper state at $R=9.5$, $R=11.2$, and $R=12.5$ a.u. also correspond to enhanced generation of the harmonics of the order 9–13. For the higher-order harmonics (15–19), the increased generation is observed at large distances (16–17.5 a.u.).

IV. CONCLUSION

In this paper, we have presented a time-dependent non-Hermitian Floquet approach for accurate calculations of HHG by the hydrogen molecular ion H_2^+ in intense laser field with the wavelength 532 nm. The procedure involves the extension of the complex-scaling generalized pseudospectral (CSGPS) technique for *nonuniform* and optimal spatial discretization of the two-center Hamiltonian and efficient non-Hermitian time propagation of the time-evolution operator. We show that high-precision time-dependent quasienergy wave functions, MPI rates, and HHG power spectra can be achieved by this method.

We have studied the dependence of the HHG spectra on the intensity of the laser field at the equilibrium internuclear separation. Our results confirm that the "simple man's model" [8] can give a reasonable estimate of the cutoff position. Moreover, we have explored the dependence of HHG spectra on the internuclear separation R at the field intensity 5×10^{13} W/cm^2. Our calculations reveal a strong dependence of HHG rates on R. At some R, the HHG production is strongly enhanced, and this phenomenon can be attributed to the resonantly enhanced multiphoton ionization of H_2^+ at these internuclear separations. The enhancement of higher harmonics (15–19) occurs at larger R. The observed phenomena in the R dependence of the HHG rates can be used for better control of the high-order harmonic generation process. Extension of the present approach to the study of HHG of multielectron diatomic molecules is in progress.

ACKNOWLEDGMENTS

This work was supported by the U.S. Department of Energy, Office of Basic Energy Science, Division of Chemical Sciences, and by the National Science Foundation. We acknowledge the Kansas Center for Advanced Scientific Computing for the use of Origin2400 supercomputer facilities.

[1] *Atoms and Molecules in Intense Fields*, edited by L. S. Cederbaum, K. C. Kulander, and N. H. March (Springer, New York, 1997).
[2] P. Salières, A. L'Huillier, P. Antoine, and M. Lewenstein, Adv. At., Mol., Opt. Phys. **41**, 83 (1999).
[3] T. Brabec and F. Krausz, Rev. Mod. Phys. **72**, 545 (2000).
[4] C. Spielmann, H. Burnett, R. Sartania, R. Koppitsch, M. Schnurer, C. Kan, M. Lenzner, P. Wobrauschek, and F. Krausz, Science **278**, 661 (1997).
[5] Z. Chang, A. Rundquist, H. Wang, M. M. Murnane, and H. C. Kapteyn, Phys. Rev. Lett. **79**, 2967 (1997).
[6] P. B. Corkum, Phys. Rev. Lett. **71**, 1994 (1993).
[7] J. L. Krause, K. J. Schafer, and K. C. Kulander, Phys. Rev. Lett. **68**, 3535 (1992).
[8] R. Kopold, W. Becker, and M. Kleber, Phys. Rev. A **58**, 4022 (1999).
[9] R. Velotta, N. Hay, M. B. Mason, M. Castillejo, and J. P. Marangos, Phys. Rev. Lett. **87**, 183901 (2001).
[10] N. Hay, R. Velotta, M. Lein, R. de Nalda, E. Heesel, M. Castillejo, and J. P. Marangos, Phys. Rev. A **65**, 053805 (2002).
[11] V. I. Usachenko and V. A. Pazdzersky, J. Phys. B **35**, 761 (2002).
[12] X. M. Tong and S. I. Chu, Phys. Rev. A **57**, 452 (1998).
[13] X. M. Tong and S. I. Chu, Phys. Rev. A **64**, 013417 (2001).
[14] X. Chu and S. I. Chu, Phys. Rev. A **63**, 023411 (2001).
[15] X. Chu and S. I. Chu, Phys. Rev. A **64**, 063404 (2001).
[16] M. Lein, N. Hay, R. Velotta, J. P. Marangos, and P. L. Knight, Phys. Rev. Lett. **88**, 183903 (2002); Phys. Rev. A **66**, 023805 (2002).
[17] M. Lein, P. P. Corso, J. P. Marangos, and P. L. Knight, Phys. Rev. A **67**, 023819 (2003).
[18] T. Zuo, S. Chelkowski, and A. D. Bandrauk, Phys. Rev. A **48**, 3837 (1993).
[19] A. Giusti-Suzor, F. H. Mies, L. F. DiMauro, E. Charron, and B. Yang, J. Phys. B **28**, 309 (1995).
[20] G. Lagmago Kamta and A. D. Bandrauk, Phys. Rev. A **70**, 011404(R) (2004).
[21] X. Chu and S. I. Chu, Phys. Rev. A **63**, 013414 (2001).
[22] S. I. Chu, Adv. At. Mol. Phys. **21**, 197 (1985); Adv. Chem. Phys. **73**, 739 (1989); S. I. Chu and D. A. Telnov, Phys. Rep. **390**, 1 (2004).
[23] T. Zuo and A. D. Bandrauk, Phys. Rev. A **52**, R2511 (1995).
[24] L. Y. Peng, D. Dundas, J. F. McCann, K. T. Taylor, and I. D. Williams, J. Phys. B **36**, L295 (2003).
[25] L. B. Madsen and M. Plummer, J. Phys. B **31**, 87 (1998).
[26] L. B. Madsen, M. Plummer, and J. F. McCann, Phys. Rev. A **58**, 456 (1998).
[27] Z. Mulyukov, M. Pont, and R. Shakeshaft, Phys. Rev. A **54**, 4299 (1996).
[28] M. Plummer and J. F. McCann, J. Phys. B **30**, L401 (1997).
[29] D. A. Telnov and S. I. Chu, J. Phys. B **37**, 1489 (2004).
[30] *Handbook of Mathematical Functions*, edited by M. Abramowitz and I. Stegun (Dover, New York, 1965).
[31] G. Yao and S. I. Chu, Chem. Phys. Lett. **204**, 381 (1993).
[32] D. R. Dion and J. O. Hirschfelder, Adv. Chem. Phys. **35**, 265 (1976).
[33] N. Moiseyev, Phys. Rep. **302**, 211 (1998).
[34] C. W. McCurdy, C. K. Stroud, and M. K. Wisinski, Phys. Rev. A **43**, 5980 (1991).
[35] M. Pont, D. Proulx, and R. Shakeshaft, Phys. Rev. A **44**, 4486 (1991).
[36] K. Codling and L. J. Frasinski, J. Phys. B **26**, 783 (1993).